Native point defects in $LaAlO_3$: A hybrid functional study

Minseok Choi,* Anderson Janotti, and Chris G. Van de Walle
Materials Department, University of California, Santa Barbara, California 93106, USA
(Received 12 July 2013; published 30 December 2013)

We investigate the electronic structure of defects in $LaAlO_3$ (LAO) and their effects on electronic properties of bulk and heterostructures. Our calculations indicate that vacancies have lower formation energies than interstitials and antisites. The La vacancy (V_{La}) and the Al vacancy (V_{Al}) are deep acceptors, while the oxygen vacancy (V_O) is a deep donor. The impact of these defects on the performance of metal-oxide-semiconductor devices is analyzed by placing the LAO band edges and defect levels with respect to the band edges of GaN, InGaAs, and Si. V_O introduces levels in the gap or in the vicinity of the semiconductor conduction band, resulting in carrier traps and/or leakage current through the gate oxide, while V_{La} and V_{Al} are sources of negative fixed charges. We also discuss how oxygen vacancies in LAO can influence the observed two-dimensional electron gas (2DEG) in $LaAlO_3/SrTiO_3$ heterostructures. We conclude that V_O in the LAO layer may provide electrons that fill compensating surface states, resulting in higher 2DEG densities, at least for modest LAO layer thicknesses.

DOI: 10.1103/PhysRevB.88.214117 PACS number(s): 61.72.J−, 61.72.Bb, 71.55.Ht

I. INTRODUCTION

$LaAlO_3$ (LAO) is an insulator with a large band gap; the reported values lie in the range of 5.6–6.2 eV.[1,2] It crystallizes in the perovskite structure and is widely used as a substrate for epitaxial growth of high-T_C superconductors and magnetic and ferroelectric thin films. There is great interest in LAO as a gate dielectric in Si-based complementary metal-oxide-semiconductor (MOS) devices due to its large band gap, high dielectric constant,[3] and good thermal stability,[4] aiming at minimizing current leakage through the gate dielectric[5,6] as the devices are scaled down in size. LAO has also been considered as a gate dielectric for III-V-based MOS devices, with the potential of enabling novel functionalities and adding flexibility to device design.[7–10] The quality of the high-κ oxide and of its interface with the semiconductor channel are critical for MOS devices. Defect-induced carrier traps and fixed charges in the oxide cause current leakage and scatter carriers in the channel.[7,11]

LAO also plays a key role in complex-oxide heterostructures. The observation of a two-dimensional electron gas (2DEG) at the $LaAlO_3/SrTiO_3$ (LAO/STO) interface[12] has triggered studies on the source of the 2DEG.[13–19] Formation of oxygen vacancies in either LAO or STO has been proposed to be important for the formation of a 2DEG at the LAO/STO interface, based on the fact that the sheet resistance shows a strong dependence on the oxygen partial pressure in the growth environment or in postgrowth anneals.[20–23] Direct evidence of the presence of oxygen vacancies is still lacking, however.

Experiments have shown the presence of defect states in the band gap of LAO. Photoluminescence (PL) spectra for 3.1-eV excitation energies (well below the band gap) of bulk single crystals reveal three emission peaks: a broad peak at ∼2.1 eV and two narrower peaks at 1.8 and 1.7 eV.[24] Electron-spin-resonance (ESR) and absorption measurements reveal a broad absorption peak at 3.0 eV in bulk single crystals grown by the Czochralski method; this peak was attributed to cation vacancies.[25] Two weaker ESR signals were also observed and attributed to an "F^+ center" (an oxygen vacancy that captured an electron) and to an "O^- center" (a cation vacancy that captured a hole, which localized to a neighboring O^{2-} ion).[25] Kanai *et al.* reported PL measurements on single crystals at temperatures of 10 and 300 K. They found peaks at 1.6–1.7, 2.0, and 2.8 eV.[26] A follow-up experiment measured the peaks at 1.6–1.7 eV in single-crystal and polycrystalline LAO and proposed a Cr impurity as a possible cause.[27] Kawabe *et al.*, finally, reported a PL peak at 2.5 eV in LAO single crystals grown with the float-zone method in a reducing atmosphere and attributed it to the oxygen deficiency.[28] In spite of the attempts at attribution, the microscopic origin of all of these signals remains uncertain.

Point defects in LAO have also been investigated by first-principles calculations.[29–34] Most of these studies were carried out using the local-density approximation (LDA) or the generalized gradient approximation (GGA) within the density-functional theory (DFT). In this approach the band gap is severely underestimated, leading to errors in defect formation energies and in the position of transition levels with respect to the band edges. Attempts have been made to correct for these errors,[30,31] but that has led to large variations in the calculated results. For example, in the case of V_O in cubic LAO (c-LAO), Luo *et al.*[30] reported a formation energy of 6.5 eV for the neutral V_O, while Yamamoto and Mizoguchi[31] reported a value of nearly 9.5 eV for the same defect. For V_O in rhombohedral LAO (r-LAO), Yamamoto and Mizoguchi[31] found a formation energy of the neutral V_O larger than 10 eV, but the LDA calculations by Mitra *et al.*[34] revealed a value of nearly 8 eV. Reported charge-state transition levels display equally large variations: Mitra *et al.* found that V_O introduces a donor level (+2/0) at ∼3 eV above the valence-band maximum (VBM), whereas Xie *et al.*[29] showed the same level at 1.8 eV above the VBM. These discrepancies in formation energies and defect levels can be mostly attributed to the treatment of the band-gap problem: Luo *et al.*[30] and Xie *et al.*[29] seem to have rigidly shifted the conduction band by the difference between the calculated and experimental band gap, while Yamamoto and Mizoguchi[31] applied a rigid shift to both the occupied gap states and the conduction band in order to match the experimental band gap. Mitra *et al.*[34] did not mention any correction.

In the present work we use DFT with a hybrid functional, an approach that has been demonstrated to result in accurate band

structures and enthalpy of formation[35–37] and has provided a reliable description of defect formation energies and defect levels in wide-band-gap semiconductors.[38–42] A systematic assessment of the performance of hybrid functionals in studies of point defects is included in Ref. 43. Hybrid functional calculations for V_O in LAO were recently reported;[33,34] in the present work, however, we address a much wider range of defects and an extensive discussion of their effects on electronic properties.

Details of the calculations are provided in Sec. II. The electronic and structural properties of each defect are described in Sec. III. The impact of defects on LAO/semiconductor MOS devices is addressed in Sec. IV A, and the relevance of oxygen vacancies in LAO for the 2DEG in LAO/STO heterostructures is discussed in Sec. IV B.

II. COMPUTATIONAL APPROACH

A. Density-functional theory

The calculations are based on DFT and the screened hybrid functional of Heyd-Scuseria-Ernzerhof (HSE),[44,45] implemented with the projector augmented-wave method[46] in the VASP code.[47] The calculated lattice parameter and band gap of LAO using the HSE and the GGA of Perdew, Burke, and Ernzerhof[48] are listed in Table I and compared with experimental values.[1,2,49]

LAO undergoes a phase transition from rhombohedral ($R\bar{3}c$) to cubic perovskite ($Pm\bar{3}m$) at 820 K.[50] We have performed bulk calculations for both phases, but our defect calculations have been performed in the cubic phase. The local bonding environment in the two phases is very similar, and one therefore expects defect energetics to be similar as well; this was indeed confirmed in the DFT-GGA study of Ref. 31. The mixing parameter in the HSE (i.e., amount of the nonlocal Fock-exchange) was set to 32%, providing a band gap of 5.9 eV for r-LAO, which is within the range of the reported experimental values, 5.6 eV (Ref. 1) and 6.2 eV (Ref. 2). For c-LAO, the calculated indirect band gap between the conduction-band minimum (CBM) at Γ and the VBM at R is 5.30 eV, and the direct gap at Γ is 5.46 eV. The calculated lattice parameters for both phases are close to the experimental values[49] (see Table I). The fact that our choice of mixing parameter produces a band gap close to the experimental value facilitates the comparison with experiment. We have verified that our qualitative conclusions, such as the appearance of hole localization, are not sensitive to the choice of mixing parameter

TABLE I. Lattice parameters and electronic band gaps of cubic and rhombohedral $LaAlO_3$ from GGA and HSE calculations and from experiment. α refers to the rhombohedral angle. The mixing parameter was set to 32% in the HSE calculations.

Property	GGA	HSE	Experiment
	Cubic		
a (Å)	3.81	3.77	3.81[a]
E_g (eV)	3.49	5.30	
	Rhombohedral		
a (Å)	5.39	5.33	5.36[a]
α (°)	60.23	60.19	60.10[a]
E_g (eV)	4.08	5.92	5.6,[b] 6.2[c]

[a]Reference 49.
[b]Reference 1.
[c]Reference 2.

The calculations for native point defects in LAO were performed for the cubic perovskite phase, using a 3 × 3 × 3 supercell containing 135 atoms. The wave functions were expanded in a plane-wave basis set with an energy cutoff of 400 eV, and integrations over the Brillouin zone were carried out using the Γ point. Atomic positions were relaxed until the Hellmann-Feynman forces were reduced to less than 0.01 eV/Å. The La vacancy (V_{La}), the Al vacancy (V_{Al}), the O vacancy (V_O), the O interstitial (O_i), the La antisite (La_{Al}), and the Al antisite (Al_{La}) were considered. Cation interstitials were not studied because they are already known to be energetically unfavorable.[29,30] In all cases, symmetry-broken configurations and spin polarization were taken into account.

B. Formation energy and transition level

The formation energy of a defect D in charge state q is defined as[51]

$$E^f(D^q) = E_{tot}(D^q) - E_{tot}(\text{LAO}) - \sum_i n_i\mu_i + q\epsilon_F + \Delta^q, \quad (1)$$

where $E_{tot}(D^q)$ is the total energy of a supercell containing a defect D in charge state q, and E_{tot}(LAO) is the total energy of perfect LAO supercell. n_i is the number of atoms of type i added to ($n_i > 0$) and/or removed from ($n_i < 0$) the perfect crystal to form the defect, and μ_i (i = La, Al, and O) are the atomic chemical potentials. ϵ_F is the Fermi level referenced to the VBM, and Δ^q is the correction term to align the electrostatic potential in the perfect bulk and defect supercells and to account for finite-cell size effects on the total energies of charged defects. Different approaches to correct for the finite size of the supercell in the case of charged defects have been proposed;[52–55] here we have adopted the approach of Freysoldt *et al.*,[56,57] which comprises a rigorous treatment of the electrostatic problem.

The charge-state transition level (q/q') is defined as the Fermi-level position below which the defect is most stable in charge state q and above which the same defect is stable in charge state q'. It can be derived from formation energies as

$$(q/q') = \frac{E^f(D^q;\epsilon_F = 0) - E^f(D^{q'};\epsilon_F = 0)}{(q' - q)}, \quad (2)$$

where $E^f(D^q;\epsilon_F = 0)$ is the defect formation energy for charge state q when ϵ_F is at the VBM. The position of the transition level in the band gap does not depend on the chemical potentials.

C. Atomic chemical potentials

The defect formation energy depends on the atomic chemical potential μ_i, which is taken with respect to the total energy per atom of the standard phase of the species i. That is, μ^0_{Sr} is referenced to the total energy per atom of Sr bulk, μ^0_{Al} is referenced to the total energy per atom of Al bulk, and μ^0_O

TABLE II. Calculated and experimental formation enthalpies for La_2O_3, Al_2O_3, and $LaAlO_3$ for the cubic (c) and rhombohedral (r) phases.

Materials	Present work (eV)	Experiment (eV)
La_2O_3	−19.35	−18.57[a]
Al_2O_3	−17.15	−17.37[b]
c-$LaAlO_3$	−18.86	
r-$LaAlO_3$	−18.83	−18.69[c]

[a]Reference 58.
[b]Reference 59.
[c]Reference 60.

is referenced to half of the total energy of an isolated O_2 molecule.

In this formalism the chemical potentials μ_i (i = La, Al, and O) are variable, yet restricted by the formation of limiting phases containing La, Al, and O. The chemical potentials μ_i must satisfy the stability condition of LAO:

$$\mu_{La} + \mu_{Al} + 3\mu_O = \Delta H_f(\text{LAO}), \quad (3)$$

with $\mu_{La} \leqslant 0$, $\mu_{Al} \leqslant 0$, and $\mu_O \leqslant 0$. ΔH_f(LAO) is the formation enthalpy of perfect LAO crystal. The chemical potentials μ_{La}, μ_{Al}, and μ_O are further constrained by the formation of La_2O_3 and Al_2O_3 phases:

$$2\mu_{La} + 3\mu_O \leqslant \Delta H_f(La_2O_3), \quad (4)$$

$$2\mu_{Al} + 3\mu_O \leqslant \Delta H_f(Al_2O_3), \quad (5)$$

where $\Delta H_f(La_2O_3)$ is the formation enthalpy of La_2O_3, and $\Delta H_f(Al_2O_3)$ is that of Al_2O_3. The calculated formation enthalpies are listed in Table II. We use Eq. (5) with a combination of Eqs. (3) and (4) to define a region in the μ_O versus μ_{Al} plane in which LAO is stable. This region is illustrated in Fig. 1.

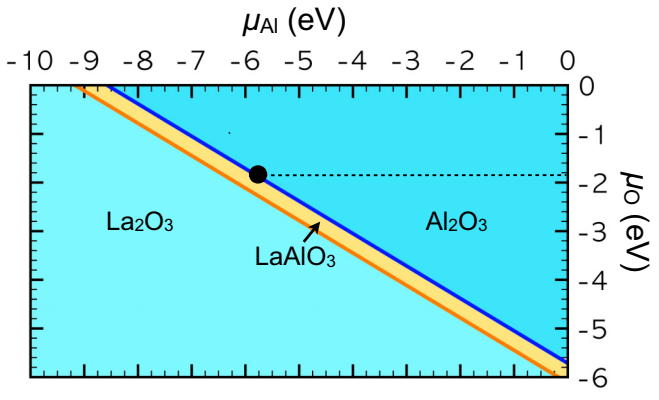

FIG. 1. (Color online) Allowed values of Al and O chemical potentials defining the stability of $LaAlO_3$. The chemical potentials μ_{La}, μ_{Al}, and μ_O are limited by the formation of the secondary phases La_2O_3 and Al_2O_3 as described in the text. The filled circle corresponds to $\mu_O = -1.84$ eV, a value chosen to represent defect energetics in $LaAlO_3$ grown by pulsed laser deposition (PLD) or molecular-beam epitaxy (MBE) (see text).

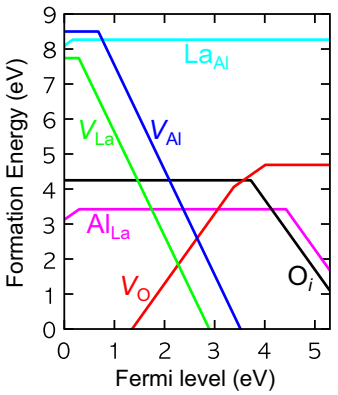

FIG. 2. (Color online) Formation energies of native point defects as a function of the Fermi level for $\mu_O = -1.84$ eV and $\mu_{Al} = -5.82$ eV, corresponding to growth or annealing conditions as discussed in the text.

LAO films as gate oxides or in heterostructures are usually grown using techniques such as atomic layer deposition (ALD),[61] pulsed laser deposition (PLD),[12,62] or molecular-beam epitaxy (MBE).[63] It is difficult to know the values of chemical potentials during growth. As an estimate for the conditions during PLD or MBE growth we set the oxygen chemical potential to $\mu_O = -1.84$ eV, corresponding to an O_2 partial pressure $P_{O_2} = 10^{-6}$ mbar at a temperature T = 1000 K. These values lie in the range of typical growth conditions for PLD or MBE (P_{O_2} =10^{-3}–10^{-7} mbar and T = 900–1100 K).[12,21 63–65] We also set μ_{Al}= −5.82 eV, which corresponds to taking Al_2O_3 as the limiting phase. These values of μ_O and μ_{Al} are indicated in Fig. 1. Postgrowth annealing at $P_{O_2} = 10^{-6}$ mbar at a temperature $T = 1000$ K in an Al-rich atmosphere would result in the same values. Taking La_2O_3 as the limiting phase (instead of Al_2O_3) would change the formation energies of La and Al vacancies by 0.6 eV.

III. RESULTS

In Fig. 2 we show the defect formation energies as a function of Fermi-level position in the band gap. The slopes of the formation-energy lines indicate the charge state of the defect, and the kinks in the lines correspond to the position of the charge-state transition levels in the gap. Figure 2 shows that the vacancies are the lower-energy defects. Oxygen vacancies are donors, while La and Al vacancies are acceptors. V_{La}^{-3} is lower in energy than V_{Al}^{-3} (by 1.8 eV); this would be true even if La_2O_3 were taken as the limiting phase, the difference in formation energy then still being 0.6 eV. In the absence of impurities, the Fermi level will be pinned by charge neutrality between positively and negatively charged defects, i.e., when the concentration of V_{La}^{-3} defects is equal to two-thirds the concentration of V_O^{+2} defects; this will occur for a Fermi level close to 2.3 eV above the VBM.

A. Oxygen vacancy

The oxygen vacancy introduces two transition levels in the upper part of the band gap: (+2/+1) at 1.92 eV and (+1/0) at 1.29 eV below the CBM. V_O is thus a deep donor, different

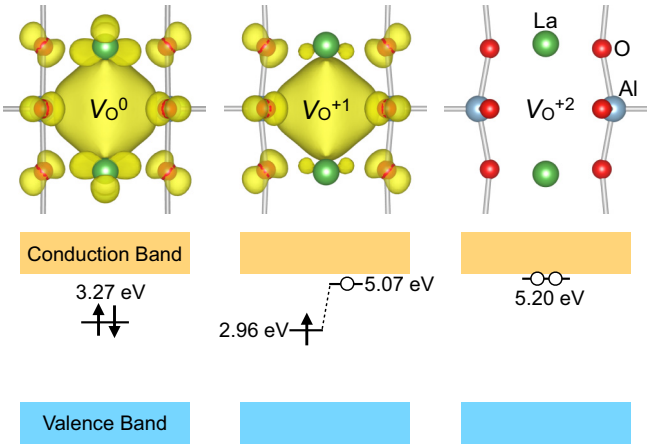

FIG. 3. (Color online) Local atomic relaxations around the oxygen vacancy in $LaAlO_3$ for (a) neutral (V_O^0), (b) singly positive (V_O^{+1}), and (c) doubly positive (V_O^{+2}) charge states. The corresponding Kohn-Sham states in the band gap, along with their occupation, are shown in the lower panels. The charge densities of the occupied gap state for V_O^0 and V_O^{+1} are also shown. The isosurfaces correspond to 10% of the maximum.[70]

from a shallow-donor behavior in other complex oxides such as $SrTiO_3$, $BaTiO_3$, $NaTaO_3$, and $KTaO_3$.[33,66–69] In the neutral charge state V_O^0, the two nearest Al atoms are displaced slightly outward from the vacancy by 0.01 Å; in the singly positive charge state V_O^{+1}, the Al atoms relax outward by 0.09 Å, and in the case of V_O^{+2} they are displaced outward by 0.14 Å. The charge (spin) density of the defect state in the gap and the local atomic relaxations are shown in Fig. 3.

Our results for V_O differ from previous GGA[29,30] as well as HSE studies.[34] Those previous studies found that V_O^{+1} is always higher in energy than either V_O^0 or V_O^{+2} (characteristic of a "negative-U" center). We attribute this to the neglect of spin polarization in these previous studies. Our calculations indicate that spin polarization lowers the formation energy of V_O^{+1} by 0.55 eV.

B. Cation vacancies

The removal of a neutral La atom leads to a deficit of three electrons; these holes can be trapped at oxygen atoms near the vacancy, in principle giving rise to the neutral, −1, −2, and −3 charge states. However, only one transition level exists in the gap: the (0/–3) level at 0.29 eV above the VBM. In the neutral charge state V_{La}^0, we find a high-spin configuration, $S = 3/2$, in which the unpaired holes are localized on separate O atoms neighboring the vacancy. Another spin-polarized configuration, $S = 1/2$, also leads to an asymmetric distribution of holes and is close in energy (within 0.01 eV). In the $S = 3/2$ configuration, the O atoms holding an unpaired hole are displaced toward the vacancy by 0.06–0.10 Å. The spin-polarized configurations are lower in energy by 1.11 eV than the (non-spin-polarized) configuration in which the three holes are equally distributed over the 12 O atoms around V_{La}. In the −3 charge state V_{La}^{-3}, there are no Kohn-Sham states in the gap. The neighboring O atoms are displaced by 0.11 Å away from the vacancy. The spin density

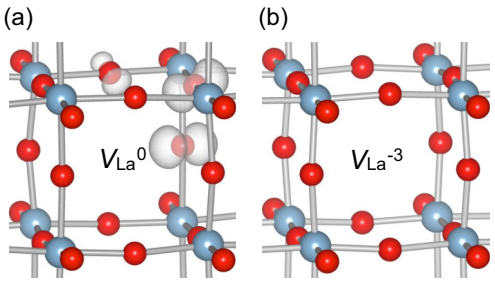

FIG. 4. (Color online) Local atomic relaxations around the La vacancy in $LaAlO_3$ for (a) neutral (V_{La}^0) and (b) negative (V_{La}^{-3}) charge states. The spin-density isosurface, representing the distribution of the unpaired holes for V_{La}^0, is also shown. The isosurfaces correspond to 10% of the maximum.[70]

and the local atomic relaxations of V_{La}^0 and V_{La}^{-3} are shown in Fig. 4.

In the case of the Al vacancy, Al–O bonds are broken and the three holes (or unpaired electrons) that are left occupy O dangling bonds. We find that the Al vacancy is a deep acceptor, with a (0/–3) level at 0.69 eV above the VBM. In the neutral charge state, the unpaired electrons are localized on separate O atoms around V_{Al} in an $S = 3/2$ configuration (see Fig. 5). This configuration is lower by 1.14 eV than the configuration in which the unpaired electrons are equally distributed over the six O atoms around V_{Al}. The $S = 1/2$ configuration of V_{Al} also shows asymmetric hole localization, but is less stable than $S = 3/2$ by 0.02 eV.

C. Oxygen interstitial

The oxygen interstitial, O_i, has a (0/–2) level at 3.72 eV above the VBM. O_i exhibits two distinct configurations, as shown in Fig. 6. In the neutral charge state, O_i forms a dumbbell configuration with an O–O bond length of 1.40 Å; a similar configuration was reported in Ref. 32. In the–2 charge state, O_i prefers to sit in an *ab* basal plane, having two La nearest neighbors with La–O distances of 2.09 Å and four O next-nearest neighbors with O–O distances of 2.37 Å. This configuration is stabilized by the Coulomb interaction between O_i^{-2} and the La ions in a +3 oxidation state. The (0/–2) level at 3.72 eV differs from previous DFT-GGA calculations, which

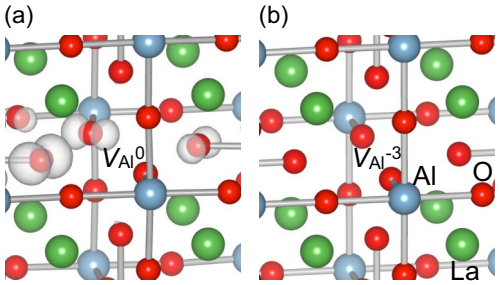

FIG. 5. (Color online) Local atomic relaxations around the Al vacancy in $LaAlO_3$ for (a) neutral (V_{Al}^0) and (b) negative (V_{Al}^{-3}) charge states. The spin-density isosurface, representing the distribution of the unpaired holes for V_{Al}^0, is also shown at the isosurface level of 10% of the maximum.[70]

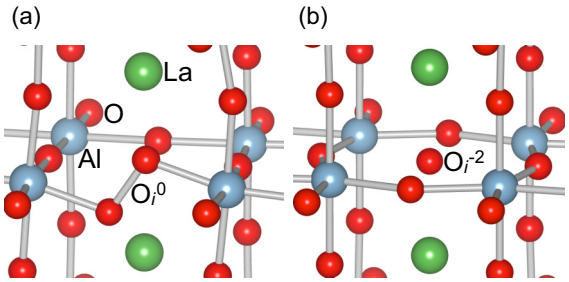

FIG. 6. (Color online) Local lattice relaxations around the oxygen interstitial in $LaAlO_3$ for the (a) neutral (O_i^0) and (b) doubly negative (O_i^{-2}) charge states. O_i^0 is most stable in a dumbbell configuration, while O_i^{-2} prefers to sit in a basal (001) plane, bonded to two out-of-plane La atoms.

found it at ∼1.7 eV (Ref. 29); we attribute this difference to the band-gap underestimation in the DFT-GGA calculations. DFT-GGA calculations by Luo *et al.* considered only the dumbbell configuration for all the charge states and reported that only O_i^{-2} is stable for the Fermi-level positions in the gap.[30]

D. Antisites

The Al_{La} ansitite has a high formation energy and leads to large local lattice relaxations, similar to the Ti antisite in $SrTiO_3$.[71] Although Al is isovalent to La in LAO, an Al atom substituting on the La site is unstable and undergoes an off-site displacement. The Al atom is displaced along the [110] direction by as much as 1 Å. Al_{La} has a (+1/0) donor level at 0.30 eV above the VBM. For a Fermi level within 0.88 eV of the CBM, Al occurs in a –2 charge state and prefers an off-site configuration along the [111] direction. The La_{Al} antisite, finally, results in transition levels (+2/+1) = 0.04 eV and (+1/0) = 0.17 eV above the VBM. The formation energy, however, is even higher than that of Al_{La}. Both antisites (Al_{La} and La_{Al}) are therefore unlikely to form in LAO.

E. Optical transitions

Finally, we comment on optical emission energies for the defects that are expected to be most prevalent, i.e., the vacancies. The stable charge states for the La and Al vacancies are −3, and that for the O vacancy is +2. These charge states are indeed most stable over a wide ranges of Fermi levels near midgap, consistent with the fact that LAO is an insulator, and the Fermi level is expected to be situated well away from the band edges—see the argument above about charge neutrality between acceptor- and donorlike defects. Based on the calculated formation energies and using the Frank-Condon principle[72] we can determine the possible optical transitions associated with these defects. Above-band-gap light (or excitation with an electron beam in cathodoluminescence) would create electron-hole pairs, and holes are rapidly captured by La or Al vacancies, changing their charge states from –3 to –2. An electron in the conduction band then recombines with the trapped hole, emitting light. The transition $V_{Al}^{-2} + e^- \rightarrow V_{Al}^{-3}$ gives rise to an emission peak at 4.1 eV, and $V_{La}^{-2} + e^- \rightarrow V_{La}^{-3}$ at 4.5 eV. For the oxygen vacancy, initially in the +2 charge state, electron-hole pair creation results in an electron being captured by V_O^{+2}, changing its charge state to +1. The transition $V_O^{+1} + h^+ \rightarrow V_O^{+2}$ results in an emission peak at 2.4 eV. This energy is close to the broad peak at 2.5 eV observed in the photoluminescence spectra of LAO single crystals.[28] This peak was found to be greatly suppressed by oxidation at 500 °C and slightly recovered by annealing in a reducing atmosphere at 1000 °C, consistent with oxygen vacancies being the source.

Note that the broad peak at ∼2.8 eV (Ref. 26) was also suggested to be due to oxygen-vacancy-related defects. This value differs from our calculated peak of 2.4 eV for the transition $V_O^{+1} + h^+ \rightarrow V_O^{+2}$. The difference may be due to the presence of impurities near V_O. Transition-metal impurities such as Cr and Fe can be unintentionally incorporated in LAO samples.[25,27] These impurities can form metal-V_O complexes,[73] affecting the electronic structure of V_O (Ref. 71) and leading to shifts in the emission peaks.

IV. DISCUSSION

A. Impact of defects on LAO gate dielectrics in MOS devices

In MOS devices, the Fermi level varies over a range that roughly encompasses the band gap of the semiconductor. Defects in the oxide, near or at the interface, can lead to carrier traps and fixed charges. These are detrimental to device performance, causing current leakage through the gate dielectric, lowering of the carrier mobility, and shift of the threshold voltage. We can determine the most likely charge state of the defect in the oxide by examining the relative position of the band edges of the oxide with respect to the band edges of the semiconductor. The impact of the defects in LAO on the electrical properties of MOS devices is thus addressed by aligning the position of defect levels in the oxide with respect to the semiconductor band edges.

The band alignment at the LAO/GaN interface was evaluated by combining the results of an explicit interface calculation and separate bulk calculations. For the interface calculation, an (001) LAO/*a*-plane GaN superlattice, containing 70 atoms, resulting in a lattice mismatch of ∼3%, is employed to obtain the lineup of averaged electrostatic potentials across the interface. Bulk calculations for c-LAO and wurtzite GaN are performed to determine the position of their VBM with respect to the averaged electrostatic potential in each material. The band offsets between GaN and other semiconductors were taken from previous calculations.[74,75] The calculated valence-band offsets with respect to LAO (illustrated in Fig. 7) are 0.9 eV for GaN, 2.8 eV for $In_{0.53}Ga_{0.47}As$, and 2.9 eV for Si. These values are in good agreement with experimental values of 1.2 eV for GaN, 2.7 eV for $In_{0.53}Ga_{0.47}As$, and 2.7 eV for Si.[76]

Figure 7 shows the position of defect levels in LAO with respect to the band edges of the semiconductors. For a Si-based MOS structure, the O-related defects V_O and O_i lead to defect levels in the vicinity of the Si band gap. The V_O (+2/+1) level occurs at 0.69 eV below the Si CBM, and the (+1/0) level occurs at 0.06 eV below the CBM, indicating that V_O leads to carrier traps and may increase leakage current. This explains the experimental observations that postdeposition annealing in O_2 lowers leakage current[61] and reduces flat-band voltage

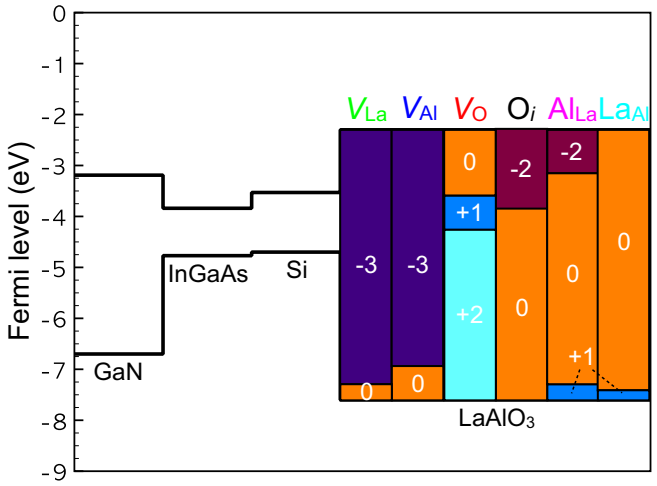

FIG. 7. (Color online) Band alignment between semiconductors (Si, $In_{0.53}Ga_{0.47}As$, GaN) and $LaAlO_3$. The positions of charge-state transition levels for native point defects in $LaAlO_3$ are shown within the $LaAlO_3$ band gap and relative to the semiconductor band edges. The zero was set at the vacuum level, with the GaN band-edge positions taken from Ref. 77.

shift and capacitance-voltage hysteresis in LAO/Si MOS structures.[78]

The O_i (0/–2) level occurs at 0.35 eV below the Si CBM. However, since the neutral and –2 charge states involve two distinct lattice configurations (Fig. 6), and for each atomic configuration individually we find no levels within the range of the Si gap, we conclude that O_i does not lead to carrier traps. O_i could still act as a negative fixed charge, for instance, in *n*-Si MOS capacitors or transistors.

V_{La} and V_{Al} are stable in the –3 charge state across the Si band gap; their transition levels occur near the LAO VBM and are therefore well below the VBM of all of the semiconductors. V_{La} and V_{Al} have modest formation energies (Fig. 2) and are likely sources of negative fixed charge.

The overall features of $In_{0.53}Ga_{0.47}As$-based MOS structures are very similar to the case of LAO/Si MOS structures. V_O plays a role as a carrier trap and may lead to leakage current, whereas V_{La}, V_{Al}, and O_i act as negative fixed-charge centers.

For *n*-channel GaN-based MOS structures, finally, the defects show similar behavior to the case of Si and InGaAs MOS structures: V_O introduces charge-state transition levels in the upper part of the GaN band gap. The (+2/+1) level of V_O lies 1.03 eV below the CBM, and the (+1/0) level is located at 0.40 eV below the CBM. Therefore V_O is a carrier trap and can cause leakage current in *n*-GaN-based MOS devices. V_{La}, V_{Al}, and O_i again act as negative fixed-charge centers in the vicinity of LAO/*n*-GaN interfaces.

B. Role of V_O in the 2DEG at $LaAlO_3/SrTiO_3$ interfaces

Growing LAO on (001) STO leads to a 2DEG at the LAO/STO interface.[12] The source of the 2DEG has been a subject of intense debate.[13–19,79] Several experimental studies have revealed that higher 2DEG densities are obtained by annealing the LAO/STO structures at lower oxygen partial pressures. This has led many groups to conclude that oxygen vacancies, acting as donors, contribute to the increase in the 2DEG density.[14,79] Most of the discussions have focused on oxygen vacancies in the STO layer; here we show that formation of oxygen vacancies in the LAO layer is more likely.

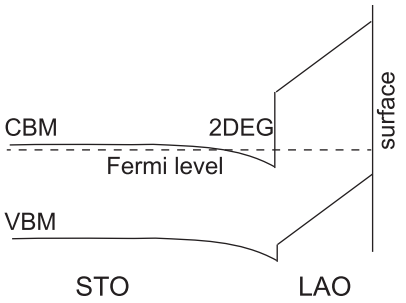

FIG. 8. Schematic band diagram of an $LaAlO_3$ (LAO) layer grown on (001) $SrTiO_3$ (STO) showing the electrostatic potential increase across the LAO layer. Toward the surface the valence-band maximum (VBM) in LAO approaches the Fermi level.

A typical band diagram of a thin LAO layer grown on STO is depicted in Fig. 8. STO is nonpolar while LAO is polar along the [001] direction. Due to the polar discontinuity, excess electrons from the LaO plane at the interface are transferred to the STO layer, forming a 2DEG.[18] Electron counting results in a 2DEG density of 0.5 electron per unit-cell area, or 3.3×10^{14} cm^{-2}. However, the observed 2DEG densities are more than an order of magnitude lower. This corresponds to a net positive charge at the interface (since ionic charge is not fully balanced by electronic charge), which results in an electric field, i.e., a buildup of electrostatic potential across the LAO layer. This potential raises the VBM toward the Fermi level, and electrons that are not accommodated at the interface fill surface states on the LAO surface.[18]

The formation energy of V_O is lowered as the Fermi level approaches the VBM in LAO (Fig. 2). Oxygen vacancies, acting as double donors, will donate electrons to passivate the LAO surface, keeping electrons from the 2DEG at the interface. Thus we conclude that forming oxygen vacancies in the LAO layer will lead to increased 2DEG densities at the LAO/STO interface, explaining the experimental observations for annealing in an O-poor atmosphere.[14,20] These results also suggest that oxidation of the surface becomes harder as the formation energy of oxygen vacancies is lowered at the surface. In addition, growing thicker LAO layers results in an increasing fraction of the LAO containing high concentrations of oxygen vacancies. These effects deteriorate the LAO quality and possibly explain why the 2DEG density saturates, rather than increases, as the LAO thickness increases beyond three or four monolayers.[13]

V. SUMMARY

We have investigated the electronic properties of point defects in LAO using hybrid density-functional calculations. The use of a hybrid functional allows for more correct calculations of formation energies and defect levels, as well as a proper description of hole localization in the case of acceptor defects. Another aspect in which the present work goes beyond previous studies is the inclusion of spin polarization. We find

that cation vacancies are deep acceptors, with defect levels near the VBM, whereas oxygen vacancies are deep donors with defects levels within 2 eV of the conduction band. Oxygen vacancies give rise to luminescence at 2.4 eV, Al vacancies at 4.1 eV, and La vacancies at 4.5 eV.

By analyzing the position of defect levels with respect to the band edges of Si, InGaAs, and GaN, we find that oxygen vacancies can act as carrier traps in LAO/semiconductor MOS devices. The La and Al vacancies will be sources of negative fixed charge in the vicinity of the interface, leading to carrier scattering. Interstitials and antisites are much higher in energy and unlikely to form.

We also find that oxygen vacancies can play a role in the formation of the 2DEG at LAO/STO interfaces. The increase in the electrostatic potential in the LAO layer results in the Fermi level being close to the VBM near the LAO surface, favoring formation of oxygen vacancies and increasing the 2DEG density.

ACKNOWLEDGMENTS

M.C. was supported by the ONR Dielectric Enhancements for Innovative Electronics Multidisciplinary University Initiative (N00014-10-1-0937). AJ was supported by the U.S. Army Research Office (W911-NF-11-1-0232). Computational resources were provided by the Center for Scientific Computing at the California Nanosystems Institute and Materials Research Laboratory (an NSF Materials Research Science and Engineering Center, DMR-1121053) (NSF CNS-0960316) and by the Extreme Science and Engineering Discovery Environment (NSF OCI-1053575).

*minseokchoi.phd@gmail.com

[1] S.-G. Lim, S. Kriventsov, T. N. Jackson, J. H. Haeni, D. G. Schlom, A. M. Balbashov, R. Uecker, P. Reiche, J. L. Freeouf, and G. Lucovsky, J. Appl. Phys. **91**, 4500 (2002).

[2] E. Cicerrella, J. L. Freeouf, L. F. Edge, D. G. Schlom, T. Heeg, J. Schubert, and S. A. Chambers, J. Vac. Sci. Technol. A **23**, 1676 (2005).

[3] G. A. Samara, J. Appl. Phys. **68**, 4214 (1990).

[4] D. O. Klenov, D. G. Schlom, H. Li, and S. Stemmer, Jpn. J. Appl. Phys. **44**, L617 (2005).

[5] W. Xiang, H. Lu, L. Yan, H. Guo, L. Liu, Y. Zhou, G. Yang, J. Jiang, H. Cheng, and Z. Chen, J. Appl. Phys. **93**, 533 (2003).

[6] L. F. Edge, D. G. Schlom, S. A. Chambers, E. Cicerrella, J. L. Freeouf, B. Hollander, and J. Schubert, Appl. Phys. Lett. **84**, 726 (2004).

[7] *Fundamentals of III-V Semiconductor MOSFETs*, edited by S. Oktyabrsky and P. D. Ye (Springer, New York, 2010).

[8] N. Goel, P. Majhi, W. Tsai, M. Warusawithana, D. G. Schlom, M. B. Santos, J. S. Harris, and Y. Nishi, Appl. Phys. Lett. **91**, 093509 (2007).

[9] N. Goel, W. Tsai, C. M. Garner, Y. Sun, P. Pianetta, M. Warusawithana, D. G. Schlom, H. Wen, C. Gaspe, J. C. Keay, M. B. Santos, L. V. Goncharova, E. Garfunkel, and T. Gustafsson, Appl. Phys. Lett. **91**, 113515 (2007).

[10] C. G. Van de Walle, M. Choi, J. Weber, J. Lyons, and A. Janotti, Microelectron. Eng. **109**, 211 (2013).

[11] J. Robertson, *New High-K Materials for CMOS Applications* (Elsevier, New York, 2011), pp. 132–176.

[12] A. Ohtomo and H. Y. Hwang, Nature (London) **427**, 423 (2004).

[13] S. Thiel, G. Hammerl, A. Schmehl, C. W. Schneider, and J. Mannhart, Science **313**, 1942 (2006).

[14] W. Siemons, G. Koster, H. Yamamoto, W. A. Harrison, G. Lucovsky, T. H. Geballe, D. H. A. Blank, and M. R. Beasley, Phys. Rev. Lett. **98**, 196802 (2007).

[15] J. Lee and A. A. Demkov, Phys. Rev. B **78**, 193104 (2008).

[16] Z. S. Popović, S. Satpathy, and R. M. Martin, Phys. Rev. Lett. **101**, 256801 (2008).

[17] R. Pentcheva and W. E. Pickett, J. Phys.: Condens. Matter **22**, 043001 (2010).

[18] A. Janotti, L. Bjaalie, L. Gordon, and C. G. Van de Walle, Phys. Rev. B **86**, 241108 (2012).

[19] H. Y. Hwang, Y. Iwasa, M. Kawasaki, B. Keimer, N. Nagaosa, and Y. Tokura, Nat. Mater. **11**, 103 (2012).

[20] M. Basletic, J. L. Maurice, C. Carretero, G. Herranz, O. Copie, M. Bibes, E. Jacquet, K. Bouzehouane, S. Fusil, and A. Barthelemy, Nature Mater. **7**, 621 (2008).

[21] A. Brinkman, M. Huijben, M. van Zalk, U. Zeitler, J. C. Maan, W. G. van der Wiel, G. Rijnders, D. H. A. Blank, and H. Hilgenkamp, Nat. Mater. **6**, 493 (2007).

[22] A. Kalabukhov, R. Gunnarsson, J. Börjesson, E. Olsson, T. Claeson, and D. Winkler, Phys. Rev. B **75**, 121404 (2007).

[23] G. Herranz, M. Basletić, M. Bibes, C. Carrétéro, E. Tafra, E. Jacquet, K. Bouzehouane, C. Deranlot, A. Hamzić, J.-M. Broto, A. Barthélémy, and A. Fert, Phys. Rev. Lett. **98**, 216803 (2007).

[24] J. Q. Chen, X. Wang, Y. H. Lu, A. R. Barman, G. J. You, G. C. Xing, T. C. Sum, S. Dhar, Y. P. Feng, Ariando, Q. H. Xu, and T. Venkatesan, Appl. Phys. Lett. **98**, 041904 (2011).

[25] D. Yamasaka, K. Tamagawa, and Y. Ohki, J. Appl. Phys. **110**, 074103 (2011).

[26] K. Kanai, E. Hirata, and Y. Ohki, Jpn. J. Appl. Phys. **47**, 7980 (2008).

[27] E. Hirata, K. Tamagawa, and Y. Ohki, Jpn. J. Appl. Phys. **49**, 091102 (2010).

[28] Y. Kawabe, A. Yamanaka, E. Hanamura, T. Kimura, Y. Takiguchi, H. Kan, and Y. Tokura, J. Appl. Phys. **88**, 1175 (2000).

[29] X. Xie, Y. Cheng, B. Xiao, and Y. Ohki, Jpn. J. Appl. Phys. **51**, 041103 (2012).

[30] X. Luo, B. Wang, and Y. Zheng, Phys. Rev. B **80**, 104115 (2009).

[31] T. Yamamoto and T. Mizoguchi, Phys. Rev. B **86**, 094117 (2012).

[32] K. Xiong, J. Robertson, and S. J. Clark, Appl. Phys. Lett. **89**, 022907 (2006).

[33] W.-J. Yin, S.-H. Wei, M. M. Al-Jassim, and Y. Yan, Phys. Rev. B **85**, 201201 (2012).

[34] C. Mitra, C. Lin, J. Robertson, and A. A. Demkov, Phys. Rev. B **86**, 155105 (2012).

[35] M. Marsman, J. Paier, A. Stroppa, and G. Kresse, J. Phys.: Condens. Matter **20**, 064201 (2008).

[36] S. J. Clark and J. Robertson, Phys. Rev. B **82**, 085208 (2010).

[37]T. M. Henderson, J. Paier, and G. E. Scuseria, Phys. Status Solidi B **248**, 767 (2011).
[38]A. Alkauskas, P. Broqvist, and A. Pasquarello, Phys. Status Solidi B **248**, 775 (2011).
[39]F. Oba, A. Togo, I. Tanaka, J. Paier, and G. Kresse, Phys. Rev. B **77**, 245202 (2008).
[40]P. Deák, B. Aradi, T. Frauenheim, E. Janzén, and A. Gali, Phys. Rev. B **81**, 153203 (2010).
[41]J. L. Lyons, A. Janotti, and C. G. Van de Walle, Phys. Rev. Lett. **108**, 156403 (2012).
[42]A. Alkauskas, J. L. Lyons, D. Steiauf, and C. G. Van de Walle, Phys. Rev. Lett. **109**, 267401 (2012).
[43] C. Freysoldt, B. Grabowski, T. Hickel, J Neugebauer, G. Kresse, A. Janotti, and C. G. Van de Walle, Rev. Mod. Phys. (in press).
[44]J. Heyd, G. E. Scuseria, and M. Ernzerhof, J. Chem. Phys. **118**, 8207 (2003).
[45]A. V. Krukau, O. A. Vydrov, A. F. Izmaylov, and G. E. Scuseria, J. Chem. Phys. **125**, 224106 (2006).
[46]P. E. Blöchl, Phys. Rev. B **50**, 17953 (1994).
[47]G. Kresse and J. Hafner, Phys. Rev. B **48**, 13115 (1993).
[48]J. P. Perdew, K. Burke, and M. Ernzerhof, Phys. Rev. Lett. **77**, 3865 (1996).
[49]C. J. Howard, B. J. Kennedy, and B. C. Chakoumakos, J. Phys.: Condens. Matter **12**, 349 (2000).
[50]M. A. Carpenter, S. V. Sinogeikin, J. D. Bass, D. L. Lakshtanov, and S. D. Jacobsen, J. Phys.: Condens. Matter **22**, 035403 (2010).
[51]C. G. Van de Walle and J. Neugebauer, J. Appl. Phys. **95**, 3851 (2004).
[52]G. Makov and M. C. Payne, Phys. Rev. B **51**, 4014 (1995).
[53]J. Shim, E.-K. Lee, Y. J. Lee, and R. M. Nieminen, Phys. Rev. B **71**, 035206 (2005).
[54]C. W. M. Castleton, A. Höglund, and S. Mirbt, Modell. Simul. Mater. Sci. Eng. **17**, 084003 (2009).
[55]S. E. Taylor and F. Bruneval, Phys. Rev. B **84**, 075155 (2011).
[56]C. Freysoldt, J. Neugebauer, and C. G. Van de Walle, Phys. Rev. Lett. **102**, 016402 (2009).
[57]C. Freysoldt, J. Neugebauer, and C. G. Van de Walle, Phys. Status Solidi B **248**, 1067 (2011).
[58]E. Cordfunke and R. Konings, Thermochim. Acta **375**, 65 (2001).
[59] M.W. Chase, Jr., *NIST-JANAF Thermochemical Tables*, 4th ed. (AIP, Washington, DC, 1998).
[60]J. Cheng and A. Navrotsky, J. Mater. Res. **18**, 2501 (2003).
[61]Y. Liu, H. Kim, J.-J. Wang, H. Li, and R. G. Gordon, ECS Trans. **16**, 471 (2008).
[62]L. Qiao, T. C. Droubay, T. Varga, M. E. Bowden, V. Shutthanandan, Z. Zhu, T. C. Kaspar, and S. A. Chambers, Phys. Rev. B **83**, 085408 (2011).
[63]Y. Segal, J. H. Ngai, J. W. Reiner, F. J. Walker, and C. H. Ahn, Phys. Rev. B **80**, 241107 (2009).
[64]C. Cancellieri, D. Fontaine, S. Gariglio, N. Reyren, A. D. Caviglia, A. Fête, S. J. Leake, S. A. Pauli, P. R. Willmott, M. Stengel, Ph. Ghosez, and J.-M. Triscone, Phys. Rev. Lett. **107**, 056102 (2011).
[65]C. Merckling, M. El-Kazzi, G. Delhaye, V. Favre-Nicolin, Y. Robach, M. Gendry, G. Grenet, G. Saint-Girons, and G. Hollinger, J. Cryst. Growth **306**, 47 (2007).
[66]M. Choi, F. Oba, Y. Kumagai, and I. Tanaka, Adv. Mater. **25**, 86 (2013).
[67]Y. Iwazaki, T. Suzuki, and S. Tsuneyuki, J. Appl. Phys. **108**, 083705 (2010).
[68]M. Choi, F. Oba, and I. Tanaka, Appl. Phys. Lett. **98**, 172901 (2011).
[69]M. Choi, F. Oba, and I. Tanaka, Phys. Rev. B **83**, 214107 (2011).
[70]K. Momma and F. Izumi, J. Appl. Cryst. **44**, 1272 (2011).
[71]M. Choi, F. Oba, and I. Tanaka, Phys. Rev. Lett. **103**, 185502 (2009).
[72]A. M. Stoneham, *Theory of Defects in Solids* (Oxford University Press, New York, 1975).
[73]P. G. Sundell, M. E. Björketun, and G. Wahnström, Phys. Rev. B **73**, 104112 (2006).
[74]J. R. Weber, A. Janotti, and C. G. Van de Walle, J. Appl. Phys. **109**, 033715 (2011).
[75]M. Choi, A. Janotti, and C. G. Van de Walle, J. Appl. Phys. **113**, 044501 (2013).
[76]Z. Q. Liu, W. K. Chim, S. Y. Chiam, J. S. Pan, and C. M. Ng, J. Appl. Phys. **110**, 093701 (2011).
[77]C. G. Van de Walle and J. Neugebauer, Nature (London) **423**, 626 (2003).
[78]L. Miotti, K. P. Bastos, C. Driemeier, V. Edon, M. C. Hugon, B. Agius, and I. J. R. Baumvol, Appl. Phys. Lett. **87**, 022901 (2005).
[79]Y. Li, S. N. Phattalung, S. Limpijumnong, J. Kim, and J. Yu, Phys. Rev. B **84**, 245307 (2011).